Reference structure tomography

David J. Brady, Nikos P. Pitsianis, and Xiaobai Sun

The Fitzpatrick Center, Department of Electrical and Computer Engineering and Department of Computer Science, Duke University, Durham, North Carolina 27708

Received October 28, 2003; revised manuscript received February 27, 2004; accepted March 1, 2004

Reference structure tomography (RST) uses multidimensional modulations to encode mappings between radiating objects and measurements. RST may be used to image source-density distributions, estimate source parameters, or classify sources. The RST paradigm permits scan-free multidimensional imaging, data-efficient and computation-efficient source analysis, and direct abstraction of physical features. We introduce the basic concepts of RST and illustrate the use of RST for multidimensional imaging based on a geometric radiation model. © 2004 Optical Society of America

OCIS codes: 110.0110.

1. INTRODUCTION

A reference structure is a modulation of radiation properties such as absorption, permittivity, and polarization. Physically, it is a material distributed in the radiation space between an object and a measurement system. It may be introduced artificially or discovered and exploited in its natural form. We consider primarily the former case. Reference structure tomography (RST) embodies the use of reference structures for object analysis. Object analysis may include imaging, by which we mean estimation of a density function over the object-embedding space; parameter estimation, as in location, orientation, size, velocity, or trajectory; or classification, as in object identity, type, or group.

Precursors to RST exist in tomography, inverse problems, and imaging systems. Conventionally, computed tomography refers to multidimensional object reconstruction from line integrals.[1] The concept has been generalized to include a variety of projective and computational systems. For example, geometric tomography determines source shapes from geometric projections,[2] and discrete tomography estimates source densities in matrix form from row and column sums.[3] RST utilizes projections mediated by reference structures.

Coded-aperture imaging is the most direct antecedent of RST.[4–12] In a coded-aperture system, a two-dimensional (2D) mask modulates projections from source points onto a detector array, and the impulse response is equal to the aperture. Deconvolution of the detected 2D signal on the aperture pattern produces a focused image. This approach is particularly attractive where lens fabrication is difficult, as in x-ray imaging. RST extends the physical interface of coded apertures to three-dimensional (3D) modulation, generalizes the logical structure of coded-aperture systems to multidimensional segmentation of the source space, and integrates projections from distributed sensor components. The use of 3D modulation extends the range of realizable transformations beyond the circulant structures of conventional coded-aperture imaging.

Heavy-ion reconstruction approaches in x-ray crystallography[13–16] are another RST precursor. Heavy-ion methods use strong scattering centers as holographic references for phase retrieval in multidimensional molecular tomography. There is little freedom in designing holographic references to improve reconstruction further because the ion positions are chemically determined. Furthermore, estimating the ion positions is a particular challenge for these methods. In the RST paradigm one can imagine creating molecular binding sites within artificial nanostructures as a means of prescribing reference structures for molecular analysis.

While we believe that the RST approach is applicable to most radiation imaging modalities, we focus particularly on optical systems. Multidimensional optical imaging usually relies on pointwise scanning. Leading technologies in scanned multidimensional microscopes include those in confocal,[17–21] multiphoton,[22] near-field[23] and optical-coherence tomography[24] systems. Conventional tomographic algorithms have been adopted successfully in optical imaging by use of high-depth-of-field interferometric imaging systems,[25–27] coded-aperture systems,[28] and focal systems.[29,30] Moreover, the use of complex 3D reference structures with volume holographic filters has emerged in scanning microscopies.[31–33] In RST we explore the potential of using reference structures for the additional purposes of accelerating data acquisition and simplifying temporal correction.

Multidimensional optical components and multidimensional object analysis are the primary physical distinguishing features of RST. Where conventional design of an optical system tends to emphasize planar modulation transverse to the propagation direction, reference structures modulate fields along the direction of propagation as well as in transverse directions. Where conventional design emphasizes mappings between object and image planes embedded in volume spaces, RST considers mappings between all points in the space embedding both the object space and the measurement space. The physical features lead to new algorithmic approaches that also distinguish RST, including emphasis on anisomorphic mappings between object and measurement spaces and on basis-state-based object analysis.

1084-7529/2004/071140-08$15.00

Preliminary RST studies have recently been reported elsewhere, including multidimensional imaging with geometric reference structure,[34,35] data-efficient sensing with coded apertures,[36] and direct estimation of object size with random reference structures.[37] We introduce and illustrate the basic RST concepts in the rest of the paper. We introduce in Section 2 geometric RST, which assumes ray propagation, and use it to illustrate the principles and approaches in the design of reference structures and the use of reference structures in object analysis. Section 3 discusses the codesign of object analysis and RST with a limited number of sensors. Some simulated experiments to illustrate the RST potential are presented in Section 4. We conclude with a discussion of these results in Section 5.

2. GEOMETRIC REFERENCE STRUCTURE TOMOGRAPHY

RST characterizes objects measured by use of radiation fields. A radiation field model describes how object information is transformed into measurements. The description of a radiation field model includes (1) the parameters that describe the field, (2) the relationship between the object and field states, (3) how the field propagates, (4) how the field is modulated by the reference structure, and (5) how the field state is transduced into a measurement state. Field parameters may be real or complex numbers and may include descriptions of polarization, spectral, and coherence properties. The relationship between the object state and the field may be local and linear or it may be quite complex. Field propagation may be described by simple projections or by wave propagation. Although all of these possibilities may be included in field models for RST, this paper focuses on a simple geometric field model. The geometric model is not universally applicable or unique, but it is quite useful and is adequate for presenting the basic concept of RST.

The geometric model makes the following assumptions:

1. The field is described by a non-negative real intensity value at each point in space.
2. The object density at each point contributes additively to the field at that point.
3. The field propagates along straight rays, and the amplitude of a ray is the sum of all object density points along the ray.
4. A reference structure can block or attenuate a field ray.
5. A measurement point sums the amplitude of all rays incident on it.

The geometric model is formalized with a visibility function or impulse response. The visibility $v(\mathbf{r}_1, \mathbf{r}_2)$ is defined on any pair of points in the object-embedding space. The visibility describes the contribution of the field at point $\mathbf{r}_2$ to the field at point $\mathbf{r}_1$. While the impulse response for a general field model may be complex or vector valued, the visibility under the geometric model is assumed to be real and non-negative. We say that $\mathbf{r}_2$ is visible from $\mathbf{r}_1$ if and only if $v(\mathbf{r}_1, \mathbf{r}_2)$ is nonzero.

We consider RST under the geometric model by using distributions describing the object state $[f(\mathbf{r})]$, the measurement state $[m(\mathbf{r})]$, and the reference structure $[\Phi(\mathbf{r})]$. If the reference structure is perfectly absorbing, $\Phi(\mathbf{r})$ may represent a surface contour of the reference structure. In other cases, such as partial absorbers, we may consider $\Phi(\mathbf{r})$ as a volume distribution. To simplify our description of the basic RST concepts we do not consider the material's properties in detail.

The reference structure distribution induces, by obscuration or absorption, a nontrivial visibility function $v(\mathbf{r}_1, \mathbf{r}_2)$. In the case of obscuration, the visibility function may take Boolean values only. In the 2D illustration in Fig. 1, we have $v(P, R) = 0$ since points P and R are invisible to each other, and $v(P, Q) = 1$ and $v(R, Q) = 1$ since Q is visible from both points P and R. In general, for any pair of points $\mathbf{r}_1$ and $\mathbf{r}_2$, $v(\mathbf{r}_1, \mathbf{r}_2)$ is 0 if and only if the line segment between $\mathbf{r}_1$ and $\mathbf{r}_2$ intersects $\Phi(\mathbf{r})$. The visibility function in this case can be simply determined by the boundary of the occlusion, i.e., the opaque reference structure $\Phi(\mathbf{r})$. Calculation of the visibility of such a model by use of level sets is discussed in Ref. 38. In the case of continuous absorption, the reference structure $\Phi(\mathbf{r})$ may be described as a density function and the visibility function may take the form

$$v(\mathbf{r}_1, \mathbf{r}_2) = \exp\left(-\int_{\mathbf{r}_1}^{\mathbf{r}_2} \Phi(\mathbf{r}) \mathrm{d}\mathbf{r} \right). \tag{1}$$

Under the assumption that the object state $f(\mathbf{r})$ and the measurement state $m(\mathbf{r})$ are linearly proportional to the radiation field at the corresponding points, the visibility defines the object-measurement mapping according to

$$m(\mathbf{r}_i) = \int_{R^3} v(\mathbf{r}_i, \mathbf{r}) f(\mathbf{r}) \mathrm{d}\mathbf{r}, \tag{2}$$

where $m(\mathbf{r}_i)$ is the state of the ith detector positioned at $\mathbf{r}_i$.

The measurement field is in all cases discretely sampled at selected locations. Transformation of Eq. (2) into discrete form introduces some clarifications and new terminology. Rather than considering a continuous visibility function, we may consider the visibility as a family of functions $v(\mathbf{r}_i, \mathbf{r})$ centered on the measurement points $\mathbf{r}_i$. The measurements may be parameterized as

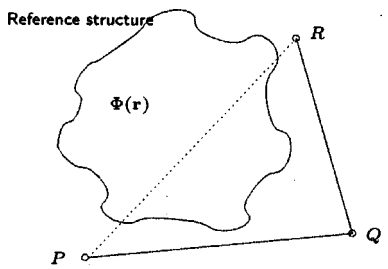

Fig. 1. Visibility modulated by an opaque geometric reference structure, $\Phi(\mathbf{r})$.

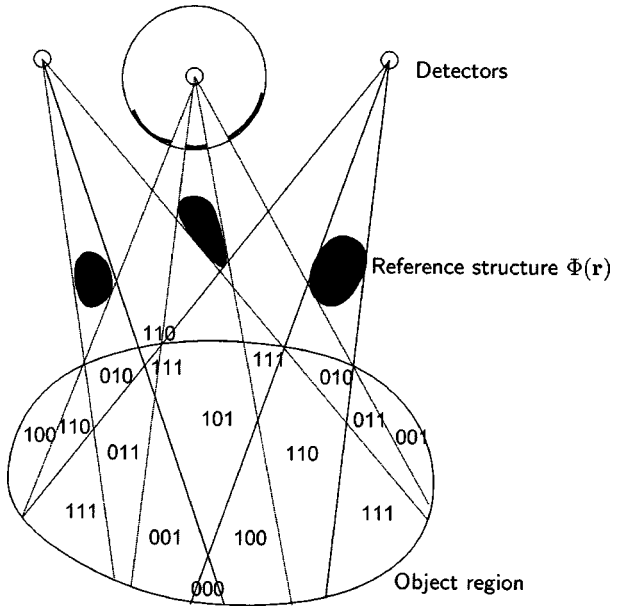

Fig. 2. Object domain, signature-cell segmentation by an opaque geometric reference structure.

$$m_i = \int_{\mathbf{S}^2} \mathrm{d}\mathbf{s} \int_0^\infty v(\mathbf{r}_i, \mathbf{r}_i + \alpha\mathbf{s}) f(\mathbf{r}_i + \alpha\mathbf{s}) \alpha^2 \mathrm{d}\alpha, \quad (3)$$

where $\mathbf{s}$ is a point on the unit sphere $\mathbb{S}^2$ centered at $\mathbf{r}_i$.

In the case of opaque reference structures, the Boolean-valued visibility function v induces a discrete partition of the object domain. Specifically, a signature vector $\chi(\mathbf{r})$ is associated with each point $\mathbf{r}$ in the object domain, indicating the visibility of the point to all the detectors. The ith element of $\chi(\mathbf{r})$ is $v(\mathbf{r}_i, \mathbf{r})$. It is equal to 1 if and only if point $\mathbf{r}$ is visible to the detector located at $\mathbf{r}_i$. Contiguous points with the same signature form a cell that we refer to as a signature cell. The object domain is partitioned into signature cells. There may be more than one cell with the same signature, as can be seen in Fig. 2.

The reference structure and the domain partition may be described geometrically as follows. Consider the case that the detectors, the reference structures, and the object domain are well separated spatially as in Fig. 2. For each sensor located at $\mathbf{r}_i$, a reference projection sphere S_i^2 centered at $\mathbf{r}_i$ of nonzero radius can be chosen so that it does not intersect the object or other spheres S_j^2. Define the local visibility function on S_i^2, $v_i(\mathbf{s}) = v(\mathbf{r}_i, \mathbf{s})$, $\mathbf{s} \in S_i^2$. It partitions the sphere S_i^2 into transparent and opaque spherical cells, corresponding to value 1 or 0. The partition of S_i^2 is the reference structure projected onto the sphere along the rays from the ith detector. Conversely, the opaque–transparent partition patterns on the reference projection spheres, i.e., the local visibility functions, specify the domain segmentation introduced by the reference structure, as illustrated by the signature cells in Fig. 2. Rays from each sensor passing through its reference projection sphere partition the object domain into regions visible or invisible to the sensor. The joint partitions from all the sensors segment the object space into signature cells. In Fig. 2 cells with signature 000 are invisible to all three sensors, and cells with signature 110 are visible to the first two sensors but invisible to the third. In RST implementation sensors and reference structure may be integrated, for example, a sensor may act as an occlusion to another sensor.

With the signature cell segmentation, the source-measurements mapping of Eq. (2) can be represented in discrete form. Let C_j be the jth cell with signature χ_j and volume v_j. Then

$$m_i = \sum_j \chi_{ij} v_j f_j, \quad (4)$$

where χ_{ij} is the ith element of signature χ_j and

$$f_j = \frac{1}{v_j} \int_{C_j} f(\mathbf{r}) \mathrm{d}\mathbf{r} \quad (5)$$

is the average of the source-distribution function over the cell C_j. Equation (4) can be written in matrix form as

$$\mathbf{m} = \mathbf{X}\mathbf{D}_\mathrm{w}\mathbf{f}, \quad (6)$$

where $\mathbf{m} = [m_i]$ is the measurement vector, $\mathbf{X} = [\chi_{ij}]$ is the signature matrix, $\mathbf{D}_\mathrm{w}$ is the diagonal weight matrix with entries of the volume vector $[v_j]$, and $\mathbf{f} = [f_j]$ is the source distribution discretized over the cells.

The sensors and reference structure will be designed with respect to the type of object analysis and the class of objects under consideration. In the case of parameter estimation, for example, $\mathbf{f}$ is a parameterized vector and Eq. (6) may be a system of nonlinear equations for the parameters. In the case of imaging, the density-distribution function $f(\mathbf{r})$ may be represented as a linear combination of prescribed basis functions $f(\mathbf{r}) = \Sigma_{j=1:K} c_j b_j(\mathbf{r})$. Equation (6) becomes the linear equation for the coefficients,

$$\mathbf{m} = \mathbf{X}\mathbf{D}_\mathrm{w}\mathbf{B}\mathbf{c}, \quad (7)$$

where the (i, j) element of $\mathbf{B}$ is the average value of basis function b_j over cell C_i; see Eq. (5). When the characteristic functions of the signature cells are used as basis function, i.e., $b_j(\mathbf{r}) = [\mathbf{r} \in C_j]$, $\mathbf{B}$ is the identity matrix. There are a few drawbacks to the use of such basis functions. Only piecewise functions on the cells can be represented exactly. The number of signature cells could grow exponentially with the number of detection points. We say that objects of interest are compressible with respect to a prescribed set of basis functions if the objects can be represented by a small number of the basis functions. In that case, the number of sensors may be made as small as K, the dimension of the prescribed basis functions, and the sensor configuration and the reference structure may be designed to make the matrix product $\mathbf{X}\mathbf{D}_\mathrm{w}\mathbf{B}$ well conditioned and well structured for efficient and robust image reconstruction. We discuss modal object analysis further in Section 3.

3. MODAL IMAGING BY REFERENCE STRUCTURE TOMOGRAPHY

Consider imaging reconstruction, i.e., the estimation of a density function over the object domain. Assume that the density function $f(\mathbf{r})$ is in a vector space of finite dimension, such as in the case of a band-limited object. The object-density function is reconstructed by solving the system of linear Eqs. (7). When the object dimension K is reasonably small, one can employ as few as K sen-

sors. The goal of reference structure design is to make the matrix product $\mathbf{X}\mathbf{D}_w\mathbf{B}$ nonsingular and well-conditioned. The ith row of $\mathbf{X}$ corresponds to the local visibility function of the ith sensor and specifies the integration of the density function over the signature cells visible to the sensor. Note that matrix $\mathbf{B}$ changes with the domain partition because the (i, j) element is the integration of the jth basis function over the i signature cell. For a well-conditioned linear problem, one may also find once and for all the inverse response in the coefficient space to the measurement at each sensor.

Let $\mathbf{Q}$ be the product of the matrices $\mathbf{X}\mathbf{D}_w\mathbf{B}$ as they have been defined in Eq. (7). The matrix $\mathbf{Q}$ is a quadrature matrix; the (i, j) element $\mathbf{Q}_{ij}$ corresponds to the definite integral of basis function B_j evaluated at the visibility domain of sensor i,

$$m_i = \int_\Omega h_i(r) f(r) \mathrm{d}r = \int_\Omega h_i(r) \sum_{j=1}^{n} c_j B_j(r) \mathrm{d}r$$

$$= \sum_{j=1}^{n} c_j \int_\Omega h_i(r) B_j(r) \mathrm{d}r,$$

where $h_i(r)$ is the visibility function from sensor i at location r and $B_j(r)$ is the jth function from a family of basis functions such that object-density function $f(r) = \Sigma_{j=1}^{n} c_j B_j(r)$.

Matrix $\mathbf{Q}$ connects the visibility partition cells on the one side and the basis functions on the other side. The representation of the object function under a selected basis either extends or limits the scope of object-reconstruction precision. The object reconstruction is limited by the number M of measurements. An important purpose of object estimation is to exploit the potential within the representation scope by using additional information about the object function. A successful RST setting represents the set of basis functions chosen adequately, and the transformation matrix $\mathbf{Q}$ is of full rank and well conditioned. In addition, the RST design should be describable by a transformation matrix $\mathbf{Q}$ that is amenable to efficient solving, but we will address this issue elsewhere.

We therefore solve for the coefficients of a compressed representation of the object-density function. It is more efficient and accurate to use matrix $\mathbf{Q}$ directly, rather than its factors, matrices $\mathbf{X}$, $\mathbf{D}_w$, and $\mathbf{B}$. Signature matrix $\mathbf{X}$ may consist of a potentially large number of columns (one column for each segmentation cell in the object region).

When the linear system is of full rank or is consistently overdetermined—that is, there are at least as many sensor measurements as basis functions—the solution result recovers the coefficients of the basis that approximate the object density. In the case of an inconsistent, overdetermined linear system due to noise in the measurements or a basis selection that does not represent the object exactly, one may seek the solution of the least-squares error.

When the dimension of object space is higher than the dimension of measurement space, Eq. (6) becomes underdetermined. An underdetermined linear system of equations has infinitely many solutions. For selection of the right solution and recovery of a good approximation of the object-density function, the dimension or scope of the solution space should be reduced by additional constraints, such as knowledge about the object that is independent of the measurements. Usually these additional constraints are based on the physical properties of the object space. Examples of such knowledge are nonnegativity constraints about the object-density function, bounds to its total energy or variability, bounds in the spectral bandwidth, etc. For instance, the nonnegativity of a density function can be imposed by the following constraints:

$$0 \leqslant \mathbf{D}_w\mathbf{B}\mathbf{c} \leqslant \mathbf{e}^T\mathbf{m}. \tag{8}$$

The inequalities define a bounded convex set when $\mathbf{B}$ is of full-column rank, which is a necessary condition to be satisfied by the reference structure design. In fact, the discretized object vector is an approximation to the original object function, in terms of a set of P piecewise-constant basis functions, each of which has its support over a signature cell. In this setting, $\mathbf{B}$ is the identity matrix. In the case when $\mathbf{f}$ is not in the column space of $\mathbf{B}$ and the linear system in Eq. (7) cannot be satisfied, the system of equations can be replaced by the inequalities

$$(1 - \tau)\mathbf{m} \leqslant \mathbf{X}\mathbf{D}_w\mathbf{B}\mathbf{c} \leqslant (1 + \tau)\mathbf{m}, \tag{9}$$

where τ is an upper bound on the relative elementwise error in the approximate representation. One may be able to obtain similar inequalities based on an absolute error bound. The set of inequalities in relation (9) defines a convex set of feasible solutions. Although it is unbounded in general because it contains the affine solution space of Eq. (7), the nonnegativity constraints and the upper bound of relation 8 make the convex cone bounded. Similarly to the ideal case, the object estimates are restricted within the conjunction of the bounded convex set defined by the nonnegativity constraints in Eq. (7) and the convex set defined by the representation approximation bounds (9).

The final estimate of the object-density function is selected on the basis of certain evaluation criteria for object reconstruction. For example, it may be desirable to select a feasible solution with the minimal reconstruction residual $\mathbf{m} - \mathbf{X}\mathbf{D}_w\mathbf{B}\mathbf{c}$ in some sense subject to the constraints described above. In the 2-norm, the estimate results in the least-squares problem of minimizing the objective function $\min_c \|\mathbf{m} - \mathbf{X}\mathbf{D}_w\mathbf{B}\mathbf{c}\|_2$ with linear constraints.

The design of an effective compressive RST setup requires the determination of the number and position of sensors and occlusions to segment the object region, and the choice of the set of functions that form a basis in which the objects can be expressed concisely and efficiently. In practical terms, RST design requires the placement of sensors and occlusions to segment the object region uniformly and in such a way that the evaluation of the basis functions in the sensor visibility regions will form a nonsingular quadrature matrix. The complexity

as well as special characteristics of the object function determine the choice of the family of functions to form a basis and its cardinality (dimension). The basis cardinality in turn determines the number of sensors required. The larger the basis cardinality, the more detail of the object can be reconstructed. However, large bases require a large number of sensors and elaborate segmentation of the object region.

The challenging issue is the choice of a minimal basis that approximates the object instances to be encountered in adequate detail. To select the proper basis, statistical knowledge of the object-density function is required. Assuming that the cardinality of the chosen basis is larger than the number of sensors M, if the rank of $\mathbf{Q}$ is not full, then the position of the sensors and occlusions is not adequate to support the chosen set of basis functions. The singular-value decomposition of the quadrature matrix $\mathbf{Q}$ is an indicator of the quality of the overall RST setup.

In summary, object estimation is determined by the RST structure, the object representation model, and the model minimizing the reconstruction deviation. The object representation model, when there is not enough *a priori* knowledge, is involved primarily in object estimation. A linear representation model may entail searching for the appropriate basis functions and selecting among or reconstructing on them and may further involve a hierarchical learning process based on measurement statistics.

4. NUMERICAL SIMULATIONS

We present image reconstruction simulations to illustrate RST implementation and considerations regarding RST design and object estimation. We consider a 2D object space observed from measurement points also in the plane through a 2D reference structure. Simulations are implemented in MATLAB. The object domain is the unit square $[-0.5, 0.5] \times [-0.5, 0.5]$. We consider M sensors located regularly around a circle of radius $R_m = \sqrt{2}$ centered at the origin. The occlusions are also regularly placed around a concentric circle of radius $R_o = 7\sqrt{2}/12$ within the sensor circle.

A sample signature cell partition introduced by such a reference structure is shown in Fig. 3. That RST setup consists of $M = 40$ sensors and 30 occlusions. The sensors are located on the circumscribed circle with their positions denoted by the open circles. The occlusions—denoted by solid circles—define the occlusion boundary lines that segment the object space, which is the square plate in the middle. Different gray-scale partitions of the object space correspond to different visibility signatures. Both sensors and occlusions are positioned at regular angular intervals that have been slightly perturbed to generate an irregular partition. The partition shown consists of 16,292 cells with 16,286 unique signatures. One major target of reference structure design is to achieve partitions with uniform average cell size and a large number of unique signatures.

We focus on reconstruction experiments in two dimensions with compressive systems, as introduced in Section 3. We start by generating a reference structure and calculating the visibility polygons for each sensor. We then calculate the integrals for each basis function on the visibility area of each sensor, thus forming matrix $\mathbf{Q}$, and similarly the integral of the object-density function to calculate the sensor measurements $\mathbf{m}$. Finally we solve the resulting least-squares optimization problem $\min_{\mathbf{c}} \|\mathbf{Qc} - \mathbf{m}\|_2$ with linear constraints $(1 - \tau)\mathbf{m} \leqslant \mathbf{Qc} \leqslant (1 + \tau)\mathbf{m}$ and $\mathbf{Bc} \geqslant 0$ and with $\tau = 0.01$ by use of a primal–dual iterative solver for quadratic programming problems with linear constraints from ILOG® CPLEX®.

The columns of matrix $\mathbf{B}$ are discretizations of the 2D Daubechies wavelet-basis-functions set. More specifically, matrix $\mathbf{B}$ is formed by the Kronecker product of discretizations of the 1D cubic, Daubechies-wavelet functions at a certain level, shifted and dilated to support the domain $[-0.5, 0.5]$.[2] We use only the compressive part of the basis set at a certain level, that is, the basis functions corresponding to the average (low-pass) set of coefficients at that level and not the functions corresponding to the detail (high-pass) set of coefficients of the same or prior levels. See Fig. 4 for a pictorial representation of the 2D cubic Daubechies wavelet basis. The choice of the wavelet basis itself has been arbitrary, and alternative wavelets or other functions that form a basis of the space spanned by the object-density functions of interest can be used. An ideal basis set can represent the intended object-density functions adequately with a small number of functions. Since such bases are problem-domain specific and can adversely influence the performance of image reconstruction, we choose a generic basis formed by the cubic Daubechies wavelet functions. In the case that a wavelet basis is chosen, matrix $\mathbf{B}$ need not be formed explicitly, as products with this matrix correspond to a 2D wavelet transform synthesis that can be calculated in linear complexity, memory space, and computational time.

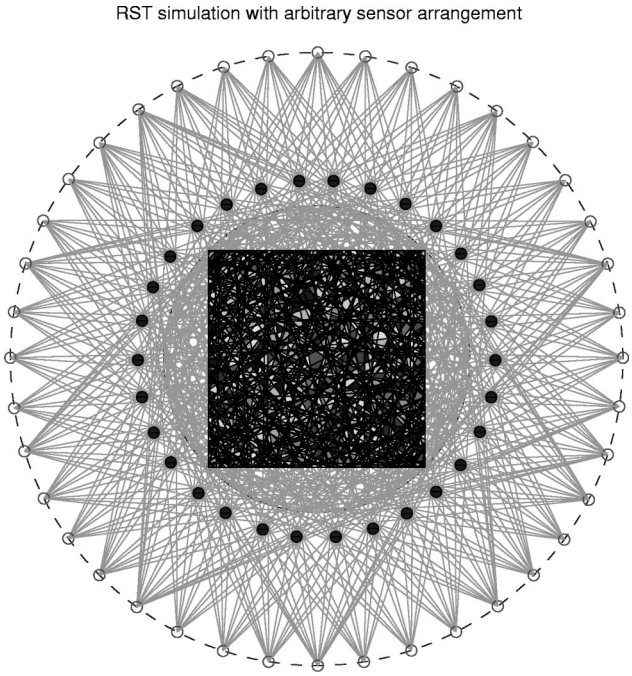

Fig. 3. Sample two-dimensional object domain partition induced by a reference structure.

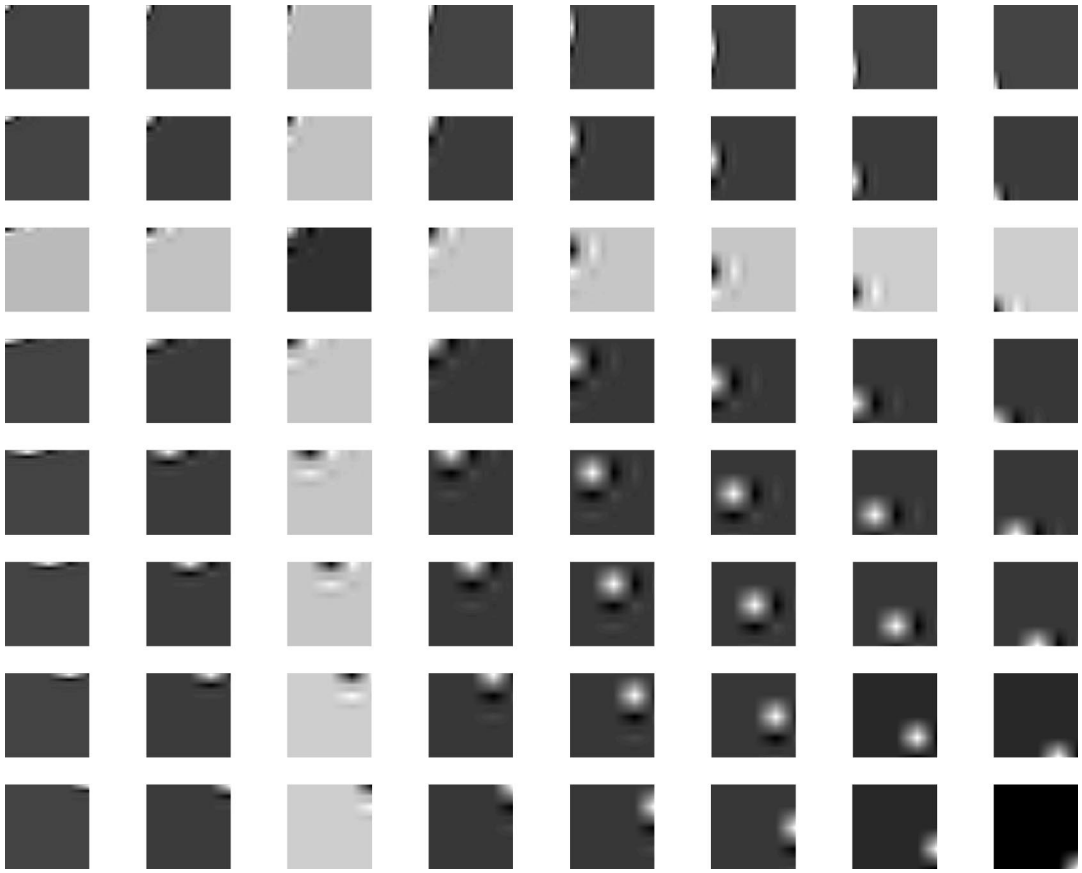

Fig. 4. Pictorial representation of the two-dimensional cubic Daubechies wavelet basis of cardinality 64. The intensity of each image has been enhanced to utilize the full gray scale and is not consistent from image to image.

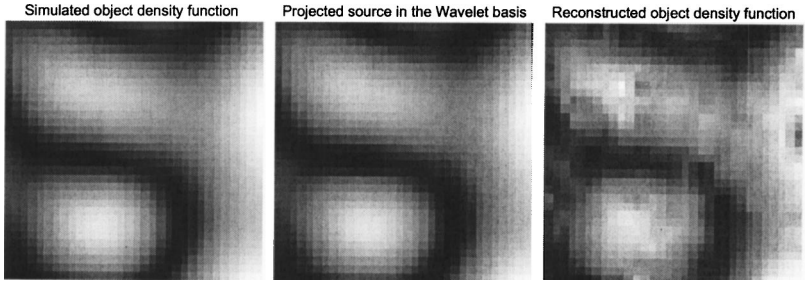

Fig. 5. Simulated band-limited object-density function used in our reconstruction; on the left is the original, in the middle is the representation in the Daubechies cubic wavelet basis, and the resulting reconstruction is on the right.

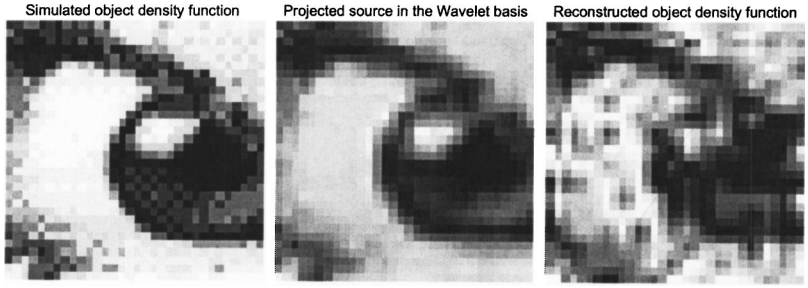

Fig. 6. Detail from the clown image used in our reconstruction; on the left is the original, in the middle is the representation in the Daubechies cubic wavelet basis, and the resulting reconstruction is on the right.

We performed two different kinds of reconstruction simulations. In the first one we reconstructed a band-limited function and in the second, we reconstructed an image fragment. The two reconstructions required different approaches in sampling and representation, so we used two different reference structure designs. The band-limited object-density function can be adequately approximated by a level 3 wavelet; thus it requires a

much smaller number of sensors than the image fragment density function. For the latter, we used a level 1 approximation wavelet basis.

The band-limited object-density function used for the first reconstruction simulation experiment is shown on the left in Fig. 5. It was generated by $f(x, y) = |\Sigma_j \Sigma_k a_{jk} \exp[-2\pi i(jx + ky)]|$. The coefficients a_{jk} were randomly generated with normal distribution. The summations were limited to six terms to simulate a band-limited function. The representation of the object-density function in the compressive Daubechies cubic-wavelet basis of level 3 is shown in the middle of Fig. 5. The reference structure setting consisted of 64 sensors and an equal number of circular occlusions. The point sensors were the vertices of a regular polygon concentric with the object region that had been slightly perturbed by a random variable of normal distribution. Similarly, all occlusions were of identical radius and appeared at equiangular positions at distance $7\sqrt{2}/12$. Note that the number of basis functions used for the sample reconstruction was also equal to the number of sensors. The subimage on the right of Fig. 5 illustrates object estimation with the minimal 2-norm residual subject to nonnegativity constraints.

The image fragment object-density function used for the second reconstruction simulation experiment is shown on the left in Fig. 6. It is a 32×32-pixel detail of the "clown" test image that comes with MATLAB. The projection of the object-density function in the compressive Daubechies cubic-wavelet basis of level 1 is shown in the middle of Fig. 6. The reference structure setting was identical in all aspects to that of the previous example (Fig. 5), the only difference being the number of sensors and circular occlusions was 324. The subimage on the right of Fig. 6 displays the reconstructed object-density function resulting from the minimization of the 2-norm residual subject to nonnegativity constraints.

One would expect that a setup with the number of sensors equal to the cardinality of the basis—assuming that it is described by a nonsingular transformation matrix—and all object states adequately expressed by the chosen basis would be reconstructible. In reality, though, we saw that the matrix $\mathbf{Q}$ could be badly conditioned owing to noise in the sensor-reading–object-density-function integration. Thus we resorted to solving an optimization problem for the image reconstruction.

5. DISCUSSION

RST introduces and utilizes known multidimensional objects to analyze unknown multidimensional objects. This work presents a simple geometric model of RST and introduces the concept of compressive measurement in tomographic systems, but does not cover the full range of RST concepts. One aspect of RST neglected here is obvious: We do not consider wave-theoretic models of the radiation fields. Another important aspect of RST left uncovered is subtler: Reference-structure-based object-space segmentation may be implemented on object-configuration spaces rather than naïve object-density spaces.

Wave-theoretic and coherence models of RST substantially increase both the complexity and the applicability of the model. Diffraction effects will limit the resolution of RST-based imaging to wavelength scales and will reduce the spatial bandwidth of object-space segmentation. Wave models also change the fundamental structure of the object-measurement mapping in cases where coherence and phase properties of the field are preserved. Such cases introduce a nonlinear mapping at the measurement interface (the measurement is generally proportional to the square of the field). This nonlinearity can be used to develop holographic models of RST.

The general problem of attempting to reconstruct an arbitrary object-density function from sensor measurements can be ill-posed and numerically ill-conditioned. However, for special cases, *a priori* knowledge of the object composition and structure can be utilized in the RST design to transform the reconstruction problem into a well-posed and well-conditioned procedure. Such abstraction to higher levels may also resolve nonlinearities implicit in the impulse-response model for object–radiation coupling. Moreover, the computational complexity of the reconstruction may be reduced substantially because of the reduction in ambiguity and the processing of higher-level abstractions in lower-dimensional spaces. In essence, RST permits the decoupling of the density estimation from target estimation. With RST we may directly estimate abstract and nonlocal object characteristics of a target with the appropriate reconstruction procedures. While these abstract measures may not be direct measures of ideal descriptors, the challenge of inverting them to obtain such measures may be substantially less than the joint challenges of object-density estimation and subsequent target estimation from image data. For instance, in many surveillance-type applications we want only to locate the position and the cardinality of a specified target without reconstructing the whole object scene. More generally, we may need to estimate only some aspects of the object, such as its position or size. Similarly, we may want only to classify an object among a set of predetermined targets, for instance, determining the shape or orientation of the object among a discrete set of shapes or orientations.

ACKNOWLEDGMENT

This work was supported through the Integrated Sensing and Processing program of the Defense Advanced Research Projects Agency's Defense Sciences Office through U.S. Army Research Office grant DAAD19-01-1-0641.

Corresponding author N. P. Pitsianis's e-mail address is nikos@cs.duke.edu.

REFERENCES

1. A. C. Kak and M. Slaney, *Principles of Computerized Tomographic Imaging* (IEEE Press, Piscataway, N.J., 1988).
2. R. Gardner, *Geometric Tomography* (Cambridge U. Press, Cambridge, UK, 1995).
3. G. Herman and A. Kuba, eds., *Discrete Tomography* (Birkhäuser, Boston, Mass., 1999).

4. E. E. Fenimore, "Coded aperture imaging—predicted performance of uniformly redundant arrays," Appl. Opt. **17**, 3562–3570 (1978).
5. A. R. Gourlay and J. B. Stephen, "Geometric coded-aperture masks," Appl. Opt. **22**, 4042–4047 (1983).
6. G. Indebetouw and W. P. Shing, "Scanning optical reconstruction of coded aperture images," Appl. Phys. B Photophys. Laser Chem. **27**, 69–76 (1982).
7. M. Matsuoka and Y. Kohmura, "A new concept of x-ray microscopes with a coded-aperture imaging mask," Jpn. J. Appl. Phys., Part 1 **34**, 372–373 (1995).
8. K. A. Nugent, "Coded-aperture imaging—a Fourier space analysis," Appl. Opt. **26**, 563–569 (1987).
9. G. K. Skinner, "Imaging with coded-aperture masks," Nucl. Instrum. Methods Phys. Res. Sect. A **221**, 33–40 (1984).
10. G. K. Skinner and T. J. Ponman, "Inverse problems in x-ray and gamma-ray astronomical imaging," Inverse Probl. **11**, 655–676 (1995).
11. R. F. Wagner, D. G. Brown, and C. E. Metz, "On the multiplex advantage of coded source aperture photon imaging," in *Digital Radiography*, W. R. Brody, ed., Proc. SPIE **314**, 72–76 (1981).
12. L. I. Yin, J. I. Trombka, and S. M. Seltzer, "Three-dimensional imaging of x-ray and gamma-ray objects in real time," Appl. Opt. **19**, 2952–2956 (1980).
13. E. de la Fortelle and G. Bricogne, "Maximum-likelihood, heavy-atom parameter refinement for multiple isomorphous replacement and multiwavelength anomalous diffraction methods," in *Macromolecular Crystallography*, Part A, Vol. 276 of Methods in Enzymology, J. Abelson, ed. (Academic, San Diego, Calif., 1997), pp. 472–494.
14. R. W. Grosse-Kunstleve and A. T. Brunger, "A highly automated heavy-atom search procedure for macromolecular structures," Acta Crystallogr. D **55**, 1568–1577 (1999).
15. U. Heinemann, G. Illing, and H. Oschkinat, "High-throughput three-dimensional protein structure determination," Curr. Opin. Biotechnol. **12**, 348–354 (2001).
16. T. V. Ohalloran, S. J. Lippard, T. J. Richmond, and A. Klug, "Multiple heavy-atom reagents for macromolecular x-ray structure determination—application to the nucleosome core particle," J. Mol. Biol. **194**, 705–712 (1987).
17. P. M. Conn, *Confocal Microscopy*, Vol. 307 of Methods in Enzymology, J. Abelson, ed. (Academic, San Diego, Calif., 1999).
18. T. R. Corle and G. S. Kino, *Confocal Scanning Optical Microscopy and Related Imaging Systems* (Academic, San Diego, Calif., 1996).
19. C. Sheppard and D. Shotton, "Confocal Laser Scanning Microscopy," No. 38 of Royal Microscopical Society Microscopy Handbooks Series (Oxford BIOS Scientific, New York, 1997).
20. D. Shotton, ed., *Electronic Light Microscopy: the Principles and Practice of Video-Enhanced Contrast, Digital Intensified Fluorescence, and Confocal Scanning Light Microscopy,* Techniques in Modern Biomedical Microscopy (Wiley-Liss, New York, 1993).
21. T. Wilson, *Confocal Microscopy* (Academic, New York, 1990).
22. W. Denk, J. H. Strickler, and W. W. Webb, "2-photon laser scanning fluorescence microscopy," Science **248**, 73–76 (1990).
23. E. Betzig, P. L. Finn, and J. S. Weiner, "Combined shear force and near-field scanning optical microscopy," Appl. Phys. Lett. **60**, 2484–2486 (1992).
24. D. Huang, E. A. Swanson, C. P. Lin, J. S. Schuman, W. G. Stinson, W. Chang, M. R. Hee, T. Flotte, K. Gregory, C. A. Puliafito, and J. G. Fujimoto, "Optical coherence tomography," Science **254**, 1178–1181 (1991).
25. D. L. Marks, R. A. Stack, and D. J. Brady, "Three-dimensional coherence imaging in the Fresnel domain," Appl. Opt. **38**, 1332–1342 (1999).
26. D. L. Marks, R. A. Stack, D. J. Brady, D. C. Munson, and R. B. Brady, "Visible cone-beam tomography with a lensless interferometric camera," Science **284**, 2164–2166 (1999).
27. P. Potuluri, M. R. Fetterman, and D. J. Brady, "High-depth-of-field microscopic imaging using an interferometric camera," Opt. Express **8**, 624–630 (2001).
28. D. L. Marks and D. J. Brady, "Three-dimensional source reconstruction with a scanned pinhole camera," Opt. Lett. **23**, 820–822 (1998).
29. M. R. Fetterman, E. Tan, L. Ying, R. A. Stack, D. L. Marks, S. Feller, E. Cull, J. M. Sullivan, D. C. Munson, S. T. Thoroddsen, and D. J. Brady, "Tomographic imaging of foam," Opt. Express **7**, 186–197 (2000).
30. D. L. Marks, R. Stack, A. J. Johnson, D. J. Brady, and D. C. Munson, "Cone-beam tomography with a digital camera," Appl. Opt. **40**, 1795–1805 (2001).
31. G. Barbastathis, M. Balberg, and D. J. Brady, "Confocal microscopy with a volume holographic filter," Opt. Lett. **24**, 811–813 (1999).
32. G. Barbastathis and D. J. Brady, "Multidimensional tomographic imaging using volume holography," Proc. IEEE **87**, 2098–2120 (1999).
33. W. H. Liu, D. Psaltis, and G. Barbastathis, "Real-time spectral imaging in three spatial dimensions," Opt. Lett. **27**, 854–856 (2002).
34. P. Potuluri, U. Gopinathan, J. R. Adleman, and D. J. Brady, "Lensless sensor system using a reference structure," Opt. Express **11**, 965–974 (2003).
35. P. Potuluri, M. Xu, and D. J. Brady, "Imaging with random 3D reference structures," Opt. Express **11**, 2134–2141 (2003).
36. U. Gopinathan, D. J. Brady, and N. P. Pitsianis, "Coded apertures for efficient pyroelectric motion tracking," Opt. Express **11**, 2142–2152 (2003).
37. A. Sinha and D. J. Brady, "Size and shape recognition using measurement statistics and random 3D reference structures," Opt. Express **11**, 2606–2618 (2003).
38. R. Tsai, P. Burchard, L.-T. Cheng, S. Osher, and G. Sapiro, "Dynamic visibility in a level set-based implicit frame work," Tech. Rep. 02-06, UCLA Computational and Applied Mathematics Reports (University of California, Los Angeles, Los Angeles, Calif., 2002).